Gating Electron–Hole Asymmetry in Twisted Bilayer Graphene

Chao-Hui Yeh,[†] Yung-Chang Lin,[†,‡] Yu-Chen Chen,[†] Chun-Chieh Lu,[†] Zheng Liu,[‡] Kazu Suenaga,[‡] and Po-Wen Chiu[†,*]

[†]Department of Electrical Engineering, National Tsing Hua University, Hsinchu 30013, Taiwan, and [‡]National Institute of Advanced Industrial Science and Technology (AIST), Tsukuba 305-8565, Japan

ABSTRACT Electron–hole symmetry is one of the unique properties of graphene that is generally absent in most semiconductors because of the different conduction and valence band structures. Here we report on the manipulation of electron–hole symmetry in the low-energy band structure of twisted bilayer graphene, where symmetric saddle points form in the conduction and valence bands as a result of interlayer coupling. By applying a gate voltage to a twisted bilayer with a critical rotation angle, enhanced electron resonance between the two saddle points can be turned on or off, depending on the electron–hole symmetry near the saddle points. The appearance of a $2D^{+}$ peak, a gate-tunable Raman feature found near the critical angle, indicates a reduction of Fermi velocity in the vicinity of the saddle point to/from which electrons are inelastically scattered by phonons in the round trip of the double-resonance process.

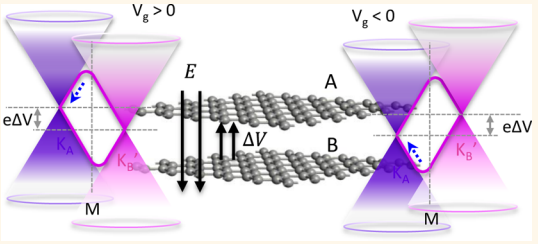

KEYWORDS: twisted bilayer graphene · saddle points · van Hove singularity · Raman

Rich and intriguing physics arise in stacks of two or more graphene layers. Particular attention has been drawn to twisted bilayer graphene (tBLG), where the crystallographic axes of the two layers are misaligned by a rotation angle θ.[1−3] Twisted graphene layers often appear in the thermal decomposition of the C-face SiC[4−6] or in the copper-assisted growth using the chemical vapor deposition (CVD) method.[7] In this two-layer system, early *ab initio* calculations of the band structure predicted that charge carriers near the crossing points of Dirac cones would behave as if the two graphene planes were isolated: the band structure consists of two rotated but noninteracting Brillouin zones where the low-energy Dirac dispersion of single-layer graphene is preserved.[8] However, later tight-binding calculations[2,9] showed more dramatic effects on the band structure. In addition to the persistence of linear dispersion near the *K* points, saddle points emerge at the crossing of Dirac cones, yielding two van Hove singularities (VHSs) in the density of states, and the Fermi velocity is remarkably renormalized in the energy window between *K* and the saddle points for small twist angles. The emergence of low-energy VHSs has been verified by scanning tunneling spectroscopy (STS),[1] angle-resolved photoemission spectroscopy (ARPES),[10] optical absorption,[11] and Raman[12−14] on both SiC- and CVD-derived tBLG. The recently observed Raman G peak enhancement effect is also attributed to the θ-dependent VHS in the density of states.[13]

Calculations using the continuum model show that tBLG is robust against gap opening at the Dirac point when subjected to a perpendicular electric field,[9,15] in sharp contrast to AB-stacked bilayer graphene, where a band gap in the shape of a Mexican hat is induced at the massive Dirac spectrum due to the symmetry breaking of constituent sublattices.[16,17] Predictions also show that the low-energy Dirac dispersion in tBLG remains unchanged upon gating, but the two Dirac cones (K_A and K_B') are shifted with respect to one another by half of the interlayer bias, forming two asymmetric saddle points in the spectrum and a finite constant density of states at low energy.[1,9,15] To experimentally explore the field-dependent symmetry of the two saddle points, we study Raman spectra of tBLG near the critical angle $\theta_c \approx 10°$, where the laser excitation energy (λ = 633 nm and E_L = 1.96 eV) is close to the energy separation of the two saddle points. We show that the interlayer coupling induces two symmetrical saddle

* Address correspondence to pwchiu@ee.nthu.edu.tw.

Received for review April 1, 2014 and accepted July 7, 2014.

Published online July 07, 2014
10.1021/nn501775h

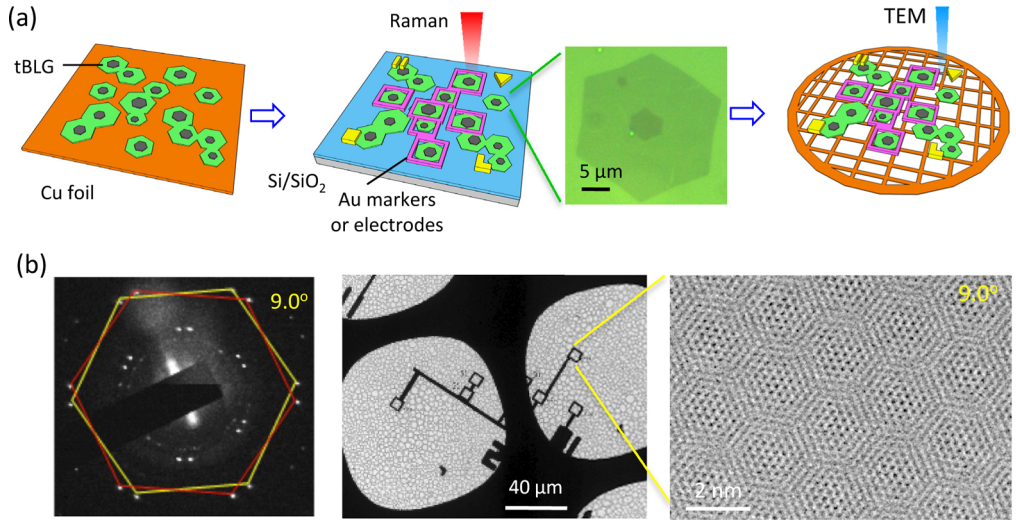

Figure 1. Schematic illustrations of the characterization technique combining Raman with TEM measurements. (a) Graphene growth on Cu foil, followed by the first wet transfer process onto the SiO_2/Si substrate. The detailed growth parameters can be found in ref 7. Markers and electrical contacts are made on the selected tBLG grains using standard e-beam lithography, followed by the second wet transfer process onto a holey TEM grid. An optical photograph of a well-shaped tBLG is shown. (b) TEM images and selected-area electron diffraction of tBLG grains. Both methods are used to determine the twist angle of tBLG.

points at the *M* point of the superlattice Brillouin zone, where enhanced resonant electron−hole pairs across the conduction and valence bands are created.[13,18] By applying an electric field through the back gate electrode, the position of the saddle points can be shifted with respect to the *M* point of the superlattice Brillouin zone in opposite directions, forming electron−hole asymmetry in the band structure of tBLG, which, in turn, switches off electron resonance between the two saddle points. To clearly see this effect, we use CVD-grown individual single-crystal tBLG. Unlike the consecutive transfer of two mechanically exfoliated graphene layers, which may suffer from physisorption of unwanted molecules at the interface and the absence of long-range atomic registry due to transfer-induced wrinkles,[19] CVD-grown tBLG has been shown to provide a better defined stacking orientation and atomic registry.[7,20]

The graphene samples studied in this work were synthesized using the atmospheric pressure CVD, which produces high-quality individual tBLG grains on 100 μm thick Cu foils (Figure 1). Previous studies showed that the number of layers can be controlled by tuning the growth parameters such as reactant gas partial pressure, temperature, and substrate thickness (also see Supporting Information).[7] It was found that the second layer usually nucleates at the center of the first layer and grows underneath.[21,22] Each layer is hexagonal in shape, with the top and bottom layers typically measuring 5−10 and 20−30 μm, respectively. To acquire the Raman spectra of tBLG upon electrostatic gating, we transfer tBLG onto a heavily doped silicon substrate with 90 nm surface oxide using bubbling transfer in a NaOH aqueous solution. The transfer process is a crucial step in this work. Bubbling transfer ensures that the tBLG is free of metal residues, which can lead to strong local screening and potential pinning. Yet, the water layer trapped between the graphene and substrate may contain excess charge-imbalanced ions, which are also problematic. To mitigate the influence of unwanted doping, the trapped water was carefully replaced by 2-propanol using capillary attraction. A standard e-beam lithography process was applied to form metal contacts (Cr/Au) on the selected tBLG. The Raman measurements were taken in the back scattering configuration. A low power intensity of <2 mW focused to a diffraction-limited spot size of ~1 μm and short acquisition time (5 s) were used to avoid laser-induced heating and damage. To provide the one-to-one correspondence of the Raman spectra and twist angle, we first take the Raman spectra of the selected tBLG grains on a silicon substrate and then determine the twist angles using electron diffraction on the free-standing state (schematically illustrated in Figure 1a). Only the well-shaped tBLG grains, such as that shown in the middle panel of Figure 1a, were selected and processed, with angles roughly predetermined by their geometries before inspection using transmission electron microscopy.

RESULTS AND DISCUSSION

When two graphene layers are stacked with a relative rotation angle θ, a periodic triangular moiré pattern appears in the local stacking, alternating between three types of order: AA, AB, and BA. The low-energy sector of the system can be well described by a continuum theory in which the two valleys are decoupled, and the Dirac points in the two layers (K_A and K_B') are offset in momentum space by $\Delta K_\theta = 2K \sin(\theta/2)$, with $K = 4\pi/3a$ (a = 2.46 Å is the lattice constant of monolayer).[9,23] In the absence of interlayer coupling,

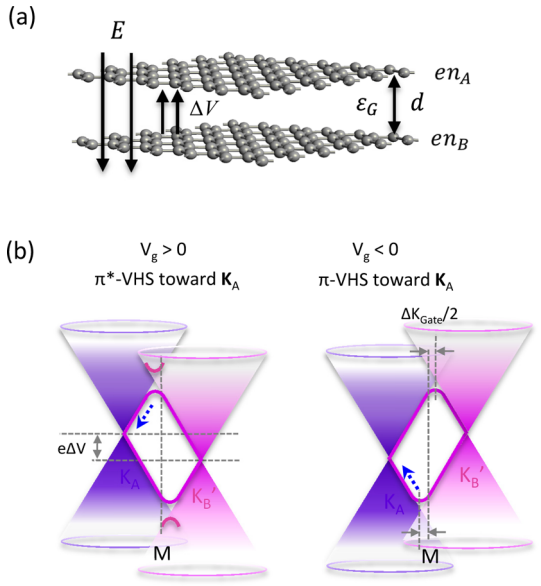

Figure 2. Effect of interlayer bias on band structure of tBLG near the Dirac points. (a) The external electric field is screened by charge imbalance Δn and by the interlayer dielectric constant ε_G. Interlayer potential difference ΔV is created by the screened electric field. (b) Energy spectrum of tBLG near the Dirac points at a potential difference ΔV. The saddle point in the conduction band moves toward K_A as a positive gate voltage V_g is applied to the gate electrode which is arranged underneath the bottom layer B. Oppositely, the saddle point in the valence band moves toward K_A as a negative gate voltage is applied.

K_A and K_B' intersect at the M point of the superlattice Brillouin zone, with a crossing point energy of $\epsilon_M(\theta) = \pm\hbar v_F \Delta K_\theta/2$. When the interlayer coupling is considered, splitting occurs at the degeneracy point, forming a pseudogap between two saddle points with VHS energies of $\epsilon_{VHS}(\theta) = \pm\epsilon_M(\theta) \mp t_\theta$, where t_θ denotes the mean interaction between states related to the two layers at ϵ_M.[15] For a large twist angle, the saddle points are distant from the Dirac cones, preserving the single-layer Dirac dispersion as evidenced by the reported ARPES and STS measurements.[24,25] As the twist angle decreases, the two Dirac cones move toward each other, and the low-energy dispersions are modified by the proximity to the saddle points. This causes a reduced Fermi velocity, which is anticipated to yield a pronounced Raman 2D blue-shift when $\epsilon_{VHS}(\theta) \approx E_L$.

In the presence of a finite interlayer bias V (Figure 2a) in the above coupled tBLG, it is predicted that the two Dirac cones (K_A and K_B') are shifted by $\pm eV/2$ with respect to the unbiased spectrum, which is qualitatively different from the case of AB-stacked BLG, where a band gap proportional to eV appears at the Dirac point.[9,15] The unique particle−hole symmetry of a nonrotated bilayer thus vanishes, as schematically illustrated in Figure 2b. The interlayer bias can be set up through the use of an external gate that is capacitively coupled to the bilayer. Application of an external electric field amounts to a varying charge density in tBLG. When a gate voltage V_g is applied between the tBLG and gate electrode (Si substrate), a potential difference develops between the graphene and gate electrode. Given that a charge density n_g is accumulated at the oxide interface of the Si side, an excess charge density $n_g = n_A + n_B$ is supplied to the bilayer and redistributed between the top and bottom layers due to the external electric field. In the limit of poor screening by the bottom layer, the excess charge density is equal in each layer and can be given by $n_A = n_B = n_g/2 = C_{ox}(V_g - V_{Dirac})/2e$ relative to half-filling of the Dirac cones, where e, C_{ox}, and V_{Dirac} are respectively the electron charge, gate capacitance, and gate voltage corresponding to the charge-neutral Dirac point. The potential difference between the two layers is

$$\Delta V = -n_g \frac{e d_G}{2\varepsilon_G} = -n_g \frac{e}{2C_G} \quad (1)$$

where d_G = 3.4 Å is the interlayer distance, and $C_G = \varepsilon_G/d_G \approx 6.8\ \mu F/cm^2$ is the interlayer capacitance per unit area.[26] Taking the interlayer screening properties into account, a charge redistribution is established between the two layers as determined by the induced free charges and the interlayer dielectric environment. The total screened electric field between the two layers is then given by $E_{tot} = (-n_g + \Delta n)e/(2\varepsilon_G)$, with a charge imbalance $\Delta n = n_B - n_A$.[26−28] The screened potential difference is

$$\Delta V = (-n_g + \Delta n)\frac{e}{2C_G} \quad (2)$$

For a bulk material with high density of states, ΔV would be effectively zero and the charge imbalance Δn would completely screen the external field, independent of the interlayer capacitance C_G. For graphene, on the contrary, the low density of states leads to an incomplete charge screening, which induces a potential difference ΔV when a gate voltage is applied. It is then expected that the energy of the two Dirac cones is shifted by $\pm e\Delta V/2$ in energy spectrum along with the two saddle points by $\pm\Delta K_{Gate}/2$ with respect to the M point of the superlattice Brillouin zone. It should be noted that the charge imbalance between the two layers can also be caused by physisorption of gas molecules on the top layer, substrate-induced doping to the bottom layer, and transfer process-induced autodoping such as metal residual or trapped excess ions between the substrate and bottom layer. Processing with care becomes critical to see the gate modulation of low-energy VHSs.

As a starting point to understanding the role of the electric-field effect on the energy spectrum, we explore the gate-dependent Raman spectra of tBLG near θ_c, where strong resonant electron−hole pairs between the π- and π^*-VHS form. Figure 3a and b, respectively, show the gating configuration and device structure. Figure 3c plots the intensity and profile evolutions of G and 2D peaks with gate voltages for $\theta \approx \theta_c - 1°$, where we expect a weaker G peak enhancement compared to

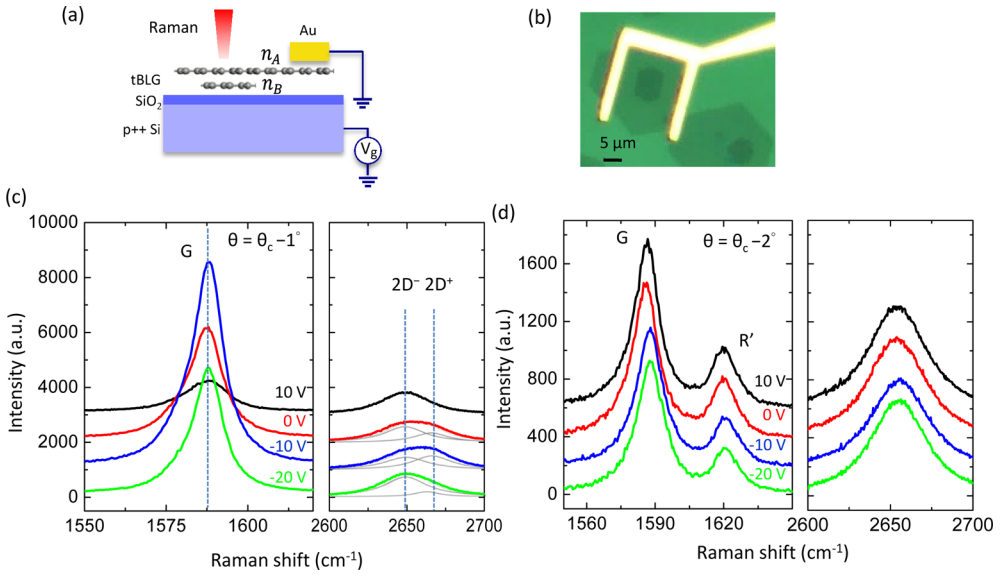

Figure 3. Device layout and Raman spectra of tBLG at $\theta \approx \theta_c - 1$. (a) Schematic of a back-gated twisted bilayer device with 90 nm SiO_2 as a gate dielectric insulator. (b) Optical photograph of a tBLG device, with a metal contact outside the bottom layer B. (c and d) Evolutions of Raman spectra with gate voltage applied to tBLG with $\theta \approx \theta_c - 1$ and $\theta \approx \theta_c - 2$, respectively. The dashed lines in (c) indicate the position of the G and 2D peaks.

that at θ_c and hence a more informative spectral change upon gating. At $V_g = 0$, the G to 2D intensity ratio is $I_G/I_{2D} \approx 5$, about a factor of 2 higher than that of nonresonant tBLG with $\theta \ll \theta_c$. It increases to the maximum, $I_G/I_{2D} \approx 10$, when a negative gate voltage ($V_g = -10$ V) is applied. This increase of G peak intensity indicates that the saddle points in the valence and conduction bands are originally not in line with the *M* point of the superlattice Brillouin zone, presumably due to the unwanted doping induced by residual sodium ions. Such a misalignment of saddle points has also been reported in the photoemission spectra of tBLG ($\theta \approx 11°$), where the charge imbalance is caused by substrate doping.[10] At a fixed Raman acquisition time, further increases or decreases of the gate voltage lead to a remarkable reduction of the G peak intensity. We see the successive quench of the G mode resonance between the two saddle points, whereas the 2D mode intensity is nearly unchanged upon gating. This change of G peak intensity is reversible in the sweep of gate voltages and is not observed in single-layer graphene (Supporting Information) and tBLG with an angle deviating far from θ_c. Figure 3d shows the same gating experiment on tBLG with twist angle of $\theta_c - 2$. A prominent R′ peak develops adjacent to the G peak. At this angle, the enhancement of G peak intensity vanishes due to the mismatch between E_L and $\epsilon_{VHS}(\theta_c - 2)$. Under this circumstance, no clear gate modulation of the G peak intensity can be seen.

One potential mechanism that might govern the modulation of G peak intensity by gating is the variation of interference between different Raman pathways involved in a single-phonon scattering process. Numbers of pathways involving different intermediate electronic states are allowed for vertical transitions (zero momentum transfer) of an electron from the valence π band to the conduction π^* band. These pathways, possessing different quantum mechanical amplitudes (phase and magnitude), will interfere with each other. Since the sum of these pathways accounts for the G peak intensity, blocking a transition pathway by changing the position of the Fermi level can result in a decrease or increase of the G peak intensity.[29] This influence of quantum coherence on peak intensity has been verified experimentally in heavily hole-doped single-layer graphene using ion-gel gating.[30] In this scenario, transition pathways that break the Pauli principle will be quenched as the Fermi energy is moved by $|\epsilon_F| > E_L/2$. However, this requires a highly effective electrostatic gating to up- or down-shift the Fermi energy ϵ_F by more than 1.0 eV for red light laser excitation (E_L = 1.96 eV). This energy is an order of magnitude higher than what can be achieved in our experimental conditions. Therefore, we exclude any significant contribution to the observed intensity modulation by coherence of Raman pathways.

Another particular feature is found in the change of the 2D peak profile. We can see an explicit two-peak structure ($2D^+$ and $2D^-$) when the G peak intensity reaches its maximum point. The high-frequency component ($2D^+$) gradually vanishes as either electron or hole density increases. This transition of the two-peak profile can also be found in the ungated tBLG near the critical angle. Figure 4 shows the evolution of the Raman spectra with the twist angle at θ_c, $\theta_c - 1°$, and $\theta_c - 2°$, highlighting the G peak intensity and 2D profile. At $\theta - \theta_c$, we see the strongest G peak enhancement effect, with an intensity ratio $I_G/I_{2D} \approx 40$. The 2D peak can be well described by a single Lorentzian with fwhm(2D) = 30 cm^{-1}. An apparent 2D

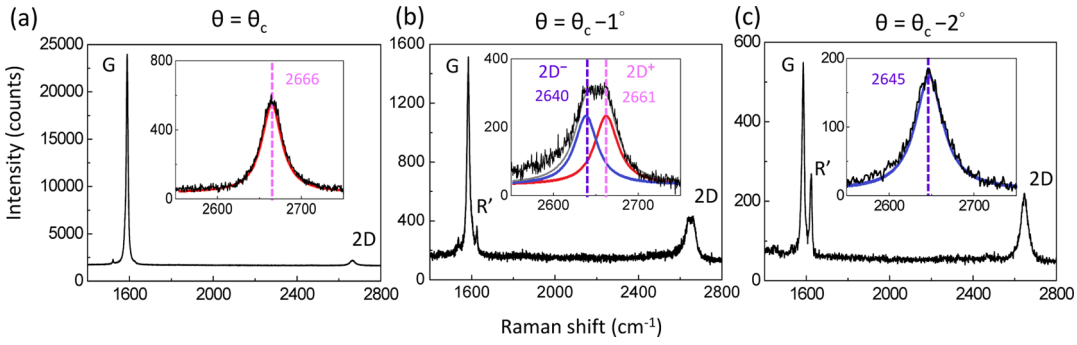

Figure 4. Raman spectra of tBLG at different twist angles. The insets highlight the 2D region with the profile fitted by $2D^+$ and $2D^-$ subpeaks for $\theta = \theta_c - 1$. The 2D peak intensity decreases with the twist angle, counterintuitive to the peak high shown in the figures.

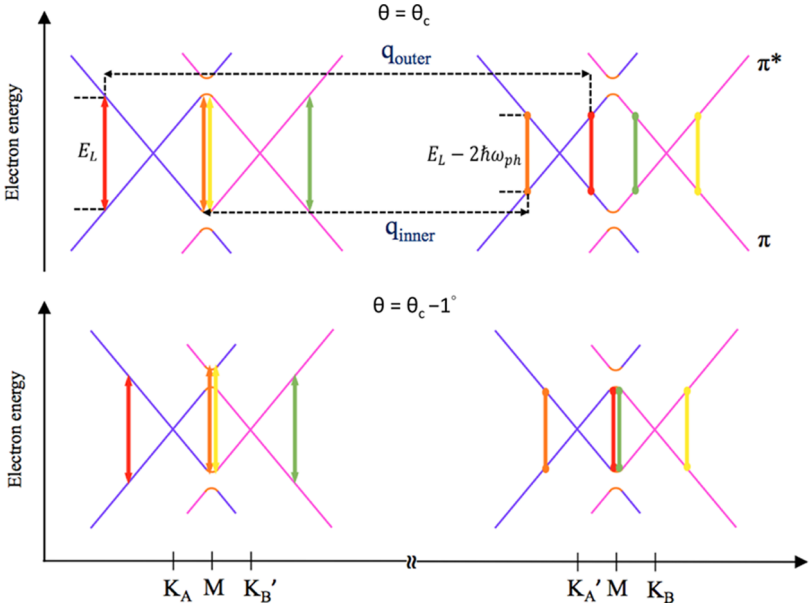

Figure 5. Double-resonance (DR) Raman processes that give rise to the 2D peak in twisted bilayer graphene near the critical angle. The transition pathways (red and orange) contribute to the 2D peak of one layer, which has the same frequency as the two pathways (yellow and green) for the other layer. Red and yellow transitions correspond to the pathway associated with "outer" phonon q_{outer}, while orange and green transitions are associated with "inner" phonon q_{inner}. At $\theta_c - 1°$, the red and green DR processes involve the phonon scattering to the electronic states near the saddle point at the π^* band. The reduced Fermi velocity in the vicinity of the saddle point leads to a significant blue-shift of the 2D peak.

blue-shift of ~20−25 cm^{-1} is another prominent feature for tBLG at θ_c. Decreasing the angle to $\theta_c - 1°$, where the energy separation between the π- and π^*-VHSs shrinks, the G peak intensity is greatly reduced, and the two-peak structure in the 2D profile develops. The profile can be described by two Lorentzian subpeaks both with fwhm(2D) = 30 cm^{-1}. Note that the appearance of the R′ peak at 1630 cm^{-1} confirms the decrease of the twist angle.[7,31] At $\theta \approx \theta_c - 2°$, the 2D profile resumes the single-peak structure. Overall, the 2D peak undergoes a transition from one peak to two peaks ($2D^+$ and $2D^-$) and then back to one peak, with intensity monotonically decreasing as the twist angle is reduced, consistent with previous reports.[13,32]

The 2D mode in graphene is activated from a double-resonance (DR) Raman scattering. It consists of an intervalley DR process that involves creation and recombination of an electron−hole pair in the vicinity of the *K* point and inelastic scattering with two in-plane transverse optical phonons around the *K* point having opposite momentum. The *k* vectors of the electronic states, excited by a laser with a wavelength spanning the range of visible light, form a triangularly distorted isoenergy contour surrounding the *K* point. Recent calculations[33] showed that "inner" and "outer" phonon scatterings between the two triangularly distorted isoenergy contours at the *K* and *K*′ points give the most important contribution to the Raman cross section of the 2D peak, forming two subpeak structures with very close frequencies. For bilayer graphene with a twist, Coh *et al.* further showed that similar two-subpeak structures develop as a result of interlayer interaction, and the peak positions vary with the twist angle, with a maximum separation of ~15 cm^{-1} occurring near θ_c.[32] In light of these results, we discuss the

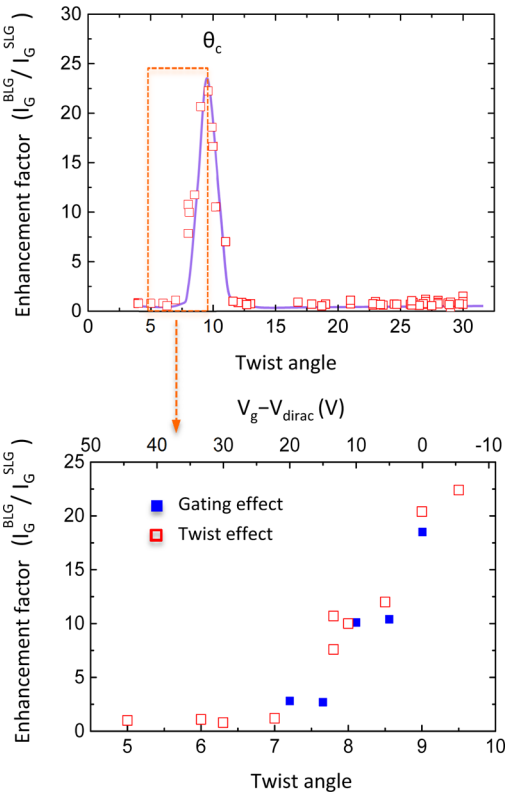

Figure 6. Upper panel shows the G peak enhancement factor (I_G^{BLG}/I_G^{SLG}) of twisted bilayer graphene as a function of twist angle under red light laser excitation. The solid line is the fit to the data. The lower panel shows the close-up of the rectangle-marked data points. The G peak enhancement factor caused by gating (data from Figure 3c) is also plotted for comparison.

origin of the two subpeaks observed in our experimental findings (Figure 3c and Figure 4b) using the framework done by Venezuela and Coh.[32,33] Figure 5 schematically illustrates the "inner" and "outer" DR processes associated with the 2D mode for tBLG at θ_c and $\theta_c - 1°$. For a laser energy of $E_L = 1.96$ eV, two "inner" and two "outer" phonons amount to the resulting 2D peak with nearly the same frequency of each contribution.[33] This accounts for the observed narrow fwhm(2D) at θ_c. At $\theta_c - 1°$, the pseudogap ($t_\theta \approx 0.2$ eV) at the band crossing compensates the decrease of ϵ_{VHS}; $\epsilon_{VHS}(\theta_c) - \epsilon_{VHS}(\theta_c - 1°) \approx 0.2$ eV, retaining one "inner" (orange) and one "outer" (yellow) phonon for the $2D^-$ subpeak. Another pair of "inner" (green) and "outer" (red) phonons causes the $2D^+$ subpeak due to the transition pathway that involves the final electronic states with significantly reduced Fermi velocity near the saddle point.[34]

The experimental findings shown above are not reflected in single-layer graphene which shares the same low-energy band structure, except for the interaction-induced band rehybridization at the crossing of the Dirac cones. The gate modulation of G peak intensity resembles the change of twist angle; that is, gating acts functionally like a "false twist". Beechem *et al.* have shown that changes in intensity can be utilized to infer variations in twist angle.[14] To account for the gate-tunable G mode resonance and the disappearance of the $2D^+$ peak upon gating, we show that the shift of saddle points is the primary cause.[1,9,15,33] We calculate the ΔK_{Gate} induced by an external field to provide a more quantitative picture. In Figure 3, we show that the G peak enhancement effect is quenched by varying the gate voltage from −10 V (maximum G intensity) to +10 V (minimum G intensity). The ΔK_{Gate} can be calculated through the relation $\Delta K_{Gate} = (\pi|n_g|)^{1/2} \approx 0.39$ nm^{-1}. Knowing the ΔK_{Gate}, we are able to convert it into an equivalent $\Delta\theta$, which shares the same effect of turning off the electron−hole resonance between the two saddle points, using the relation $\Delta K_{Gate} = 2K \sin(\Delta\theta/2)$. Thus, we obtain $\Delta\theta \approx 1.3°$. The twist angle is virtually changed from $\theta_c - 1°$ to $\theta_c - 2.3°$ when we change the gate voltage from −10 V to +10 V. In Figure 6, we compare the G peak enhancement factor as a function of twist angle for $\theta < \theta_c - 1°$ with the G peak enhancement factor as a function of gate voltage for $V < V_g - V_{Dirac}$. It can be seen explicitly that the two sets of experimental data follow a similar tendency of decrease. If the two sets of data are collapsed into a single curve, we see that a voltage change of $\Delta V_g = 20$ V corresponds to a "false twist" of about 1.7°, in reasonable agreement with the calculation discussed above.

CONCLUSIONS

In conclusion, tBLG exhibits abundant θ-dependent Raman properties that map its characteristic superlattice electronic structure. Unlike AB-stacked bilayer, which supports the induction of a band gap when subjected to a perpendicular electric field, tBLG causes an appreciable electron−hole asymmetry to appear in the electronic states near the saddle points. In addition to the intrinsic interest of altering the electronic properties of materials, the availability of a field-adjustable electron−hole resonance may open up the development of a much wider range of applications for graphene in optoelectronic devices.

METHODS

Graphene Synthesis. Single-crystal bilayer graphene was synthesized by the atmospheric pressure CVD of methane on 100 μm thick copper foils. Prior to the growth, the foil substrates were cleansed by acetone and isopropyl alcohol in order to remove unwanted organic impurities adsorbed on the copper surface. Following this cleaning, Cu foils were etched by acetic acid (CH_3COOH) at 80 °C for 30 min to clean up the native

surface oxides. The as-cleaned Cu foils were then introduced into the CVD chamber, and the furnace temperature was ramped up to 1050 °C over 20 min, with a constant flow of Ar (300 sccm) and H_2 forming gas (10 sccm). After a 40 min annealing at 1050 °C, an argon-diluted methane gas with a concentration of approximately 60 ppm was introduced and mixed with the preexisting Ar (300 sccm) and H_2 gases (15 sccm). After 15 min under these conditions, methane flow was stopped and, at the same time, Cu foils were moved to the rapid cooling zone, keeping them in the Ar/H_2 atmosphere until the samples were cooled.

Graphene Transfer. To assist tBLG transfer, polycarbonate (PC) dissolved in chloroform was used. A few drops of PC were spin coated on top of the Cu foil containing tBLG grains. The samples were then dipped into a NaOH (1 M) aqueous solution, where bubbling transfer was carried out. After the successful liftoff of the polymer scaffold, attached with tBLG grains, the samples were intensively rinsed with DI water and isopropyl alcohol so as to remove any ionic residuals from the transfer process. Finally, the tBLG grains were transferred onto 90 nm thick SiO_2 chips with the highly conductive substrate as a back gate. The remaining scaffolding polymer was removed by chloroform.

Device Fabrication. Using standard e-beam lithography, contacts were patterned only on the first (top) layer of the selected tBLG to allow the second (bottom) layer to remain free of any metal disturbance. Cr/Au was then deposited, using standard thermal evaporation and liftoff processes.

Raman Spectroscopy. A micro Raman spectrometer (Horiba Jobim-Yvon HR800) equipped with motorized X−Y sample stages was used to acquire the tBLG spectra. A 100× objective was used to provide a diffraction-limited spot size for the 633 nm red light laser. Acquisition time was limited to 5 s to minimize laser-induced heating. A Keithley 2400 voltage source was connected to the back gate of the devices and provided a fixed gate voltage during the acquisition of a Raman spectrum.

Transmission Electron Microscopy. A field emission TEM JEM-2010F (JEOL) equipped with a CEOS postspecimen spherical aberration corrector (Cs corrector) was operated at 120 kV for the TEM observations. A Gatan 894 CCD camera was used for digital recording of the SAED patterns and HR-TEM images.

Conflict of Interest: The authors declare no competing financial interest.

Acknowledgment. Z.L. and K.S. acknowledge support from JST Research Acceleration program. P.C. acknowledges Dr. Mei-Yin Chou for useful discussions. The other authors also acknowledge the project support from Taiwan Ministry of Science and Technology (NSC 100-2112-M-007-014-MY3).

Supporting Information Available: Additional CVD growth of bilayer graphene and characterization using combined Raman and TEM technique. This material is available free of charge *via* the Internet at http://pubs.acs.org.

REFERENCES AND NOTES

1. Li, G. H.; Luican, A.; Lopes dos Santos, J. M. B.; Neto, A. H. C.; Reina, A.; Kong, J.; Andrei, E. Y. Observation of van Hove Singularities in Twisted Graphene Layers. *Nat. Phys.* **2010**, *6*, 109–113.
2. Trambly de Laissardiere, G.; Mayou, D.; Magaud, L. Localization of Dirac Electrons in Rotated Graphene Bilayers. *Nano Lett.* **2010**, *10*, 804–808.
3. Wang, Z. F.; Liu, F.; Chou, M. Y. Fractal Landau-Level Spectra in Twisted Bilayer Graphene. *Nano Lett.* **2012**, *12*, 3833–3838.
4. Berger, C.; Song, Z. M.; Li, X. B.; Wu, X. S.; Brown, N.; Naud, C.; Mayou, D.; Li, T. B.; Hass, J.; Marchenkov, A. N.; *et al.* Electronic Confinement and Coherence in Patterned Epitaxial Graphene. *Science* **2006**, *312*, 1191–1196.
5. de Heer, W. A.; Berger, C.; Wu, X. S.; First, P. N.; Conrad, E. H.; Li, X. B.; Li, T. B.; Sprinkle, M.; Hass, J.; Sadowski, M. L. *et al.* Epitaxial Graphene. *Solid State Commun.* **2007**, *143*, 92–100.
6. Ohta, T.; Bostwick, A.; Seyller, T.; Horn, K.; Rotenberg, E. Controlling the Electronic Structure of Bilayer Graphene. *Science* **2006**, *313*, 951–954.
7. Lu, C. C.; Lin, Y. C.; Liu, Z.; Yeh, C. H.; Suenaga, K.; Chiu, P. W. Twisting Bilayer Graphene Superlattices. *ACS Nano* **2013**, *7*, 2587–2594.
8. Hass, J.; Varchon, F.; Millan-Otoya, J. E.; Sprinkle, M.; Sharma, N.; De Heer, W. A.; Berger, C.; First, P. N.; Magaud, L.; Conrad, E. H. Why Multilayer Graphene on 4H-SiC(000$\bar{1}$) Behaves Like a Single Sheet of Graphene. *Phys. Rev. Lett.* **2008**, *100*, 125504.
9. Lopes dos Santos, J. M. B.; Peres, N. M. R.; Castro, A. H. Graphene Bilayer with a Twist: Electronic Structure. *Phys. Rev. Lett.* **2007**, *99*, 256802.
10. Ohta, T.; Robinson, J. T.; Feibelman, P. J.; Bostwick, A.; Rotenberg, E.; Beechem, T. E. Evidence for Interlayer Coupling and Moire Periodic Potentials in Twisted Bilayer Graphene. *Phys. Rev. Lett.* **2012**, *109*, 186807.
11. Robinson, J. T.; Schmucker, S. W.; Diaconescu, C. B.; Long, J. P.; Culbertson, J. C.; Ohta, T.; Friedman, A. L.; Beechem, T. E. Electronic Hybridization of Large-Area Stacked Graphene Films. *ACS Nano* **2013**, *7*, 637–644.
12. Havener, R. W.; Zhuang, H. L.; Brown, L.; Hennig, R. G.; Park, J. Angle-Resolved Raman Imaging of Interlayer Rotations and Interactions in Twisted Bilayer Graphene. *Nano Lett.* **2012**, *12*, 3162–3167.
13. Kim, K.; Coh, S.; Tan, L. Z.; Regan, W.; Yuk, J. M.; Chatterjee, E.; Crommie, M. F.; Cohen, M. L.; Louie, S. G.; Zettl, A. Raman Spectroscopy Study of Rotated Double-Layer Graphene: Misorientation-Angle Dependence of Electronic Structure. *Phys. Rev. Lett.* **2012**, *108*, 246103.
14. Beechem, T. E.; Ohta, T.; Diaconescu, B.; Robinson, J. T. Rotational Disorder in Twisted Bilayer Graphene. *ACS Nano* **2014**, *8*, 1655–1663.
15. San-Jose, P.; Prada, E. Helical Networks in Twisted Bilayer Graphene under Interlayer Bias. *Phys. Rev. B* **2013**, *88*, 121408(R).
16. Zhang, Y. B.; Tang, T. T.; Girit, C.; Hao, Z.; Martin, M. C.; Zettl, A.; Crommie, M. F.; Shen, Y. R.; Wang, F. Direct Observation of a Widely Tunable Bandgap in Bilayer Graphene. *Nature* **2009**, *459*, 820–823.
17. Oostinga, J. B.; Heersche, H. B.; Liu, X. L.; Morpurgo, A. F.; Vandersypen, L. M. K. Gate-Induced Insulating State in Bilayer Graphene Devices. *Nat. Mater.* **2008**, *7*, 151–157.
18. Sato, K.; Saito, R.; Cong, C. X.; Yu, T.; Dresselhaus, M. S. Zone Folding Effect in Raman G-Band Intensity of Twisted Bilayer Graphene. *Phys. Rev. B* **2012**, *86*, 125414.
19. Lin, J. H.; Fang, W. J.; Zhou, W.; Lupini, A. R.; Idrobo, J. C.; Kong, J.; Pennycook, S. J.; Pantelides, S. T. AC/AB Stacking Boundaries in Bilayer Graphene. *Nano Lett.* **2013**, *13*, 3262–3268.
20. Yu, Q. K.; Jauregui, L. A.; Wu, W.; Colby, R.; Tian, J. F.; Su, Z. H.; Cao, H. L.; Liu, Z. H.; Pandey, D.; Wei, D. G.; *et al.* Control and Characterization of Individual Grains and Grain Boundaries in Graphene Grown by Chemical Vapour Deposition. *Nat. Mater.* **2011**, *10*, 443–449.
21. Li, Q. Y.; Chou, H.; Zhong, J. H.; Liu, J. Y.; Dolocan, A.; Zhang, J. Y.; Zhou, Y. H.; Ruoff, R. S.; Chen, S. S.; Cai, W. W. Growth of Adlayer Graphene on Cu Studied by Carbon Isotope Labeling. *Nano Lett.* **2013**, *13*, 486–490.
22. Fang, W.; Hsu, A. L.; Caudillo, R.; Song, Y.; Birdwell, A. G.; Zakar, E.; Kalbac, M.; Dubey, M.; Palacios, T.; Dresselhaus, M. S.; *et al.* Rapid Identification of Stacking Orientation in Isotopically Labeled Chemical-Vapor Grown Bilayer Graphene by Raman Spectroscopy. *Nano Lett.* **2013**, *13*, 1541–1548.
23. Mele, E. J. Commensuration and Interlayer Coherence in Twisted Bilayer Graphene. *Phys. Rev. B* **2010**, *81*, 161405(R).
24. Sprinkle, M.; Siegel, D.; Hu, Y.; Hicks, J.; Tejeda, A.; Taleb-Ibrahimi, A.; Le Fevre, P.; Bertran, F.; Vizzini, S.; Enriquez, H.; *et al.* First Direct Observation of a Nearly Ideal Graphene Band Structure. *Phys. Rev. Lett.* **2009**, *103*, 226803.
25. Miller, D. L.; Kubista, K. D.; Rutter, G. M.; Ruan, M.; de Heer, W. A.; First, P. N.; Stroscio, J. A. Observing the Quantization of Zero Mass Carriers in Graphene. *Science* **2009**, *324*, 924–927.

26. Sanchez-Yamagishi, J. D.; Taychatanapat, T.; Watanabe, K.; Taniguchi, T.; Yacoby, A.; Jarillo-Herrero, P. Quantum Hall Effect, Screening, and Layer-Polarized Insulating States in Twisted Bilayer Graphene. *Phys. Rev. Lett.* **2012**, *108*, 076601.
27. Castro, E. V.; Novoselov, K. S.; Morozov, S. V.; Peres, N. M. R.; Lopes dos Santos, J. M. B.; Nilsson, J.; Guinea, F.; Geim, A. K.; Neto, A. H. C. Electronic Properties of a Biased Graphene Bilayer. *J. Phys.: Condens. Matter* **2010**, *22*, 175503.
28. Gava, P.; Lazzeri, M.; Saitta, A. M.; Mauri, F. Ab Initio Study of Gap Opening and Screening Effects in Gated Bilayer Graphene. *Phys. Rev. B* **2009**, *79*, 165431.
29. Basko, D. M. Calculation of the Raman G Peak Intensity in Monolayer Graphene: Role of Ward Identities. *New J. Phys.* **2009**, *11*, 095011.
30. Chen, C. F.; Park, C. H.; Boudouris, B. W.; Horng, J.; Geng, B. S.; Girit, C.; Zettl, A.; Crommie, M. F.; Segalman, R. A.; Louie, S. G.; *et al*. Controlling Inelastic Light Scattering Quantum Pathways in Graphene. *Nature* **2011**, *471*, 617–620.
31. Carozo, V.; Almeida, C. M.; Ferreira, E. H. M.; Cancado, L. G.; Achete, C. A.; Jorio, A. Raman Signature of Graphene Superlattices. *Nano Lett.* **2011**, *11*, 4527–4534.
32. Coh, S.; Tan, L. Z.; Louie, S. G.; Cohen, M. L. Theory of the Raman Spectrum of Rotated Double-Layer Graphene. *Phys. Rev. B* **2013**, *88*, 165431.
33. Venezuela, P.; Lazzeri, M.; Mauri, F. Theory of Double-Resonant Raman Spectra in Graphene: Intensity and Line Shape of Defect-Induced and Two-Phonon Bands. *Phys. Rev. B* **2011**, *84*, 035433.
34. Ni, Z. H.; Wang, Y. Y.; Yu, T.; You, Y. M.; Shen, Z. X. Reduction of Fermi Velocity in Folded Graphene Observed by Resonance Raman Spectroscopy. *Phys. Rev. B* **2008**, *77*, 235403.